NANO LETTERS

pubs.acs.org/NanoLett Letter

Visualizing Quantum Coherence Based on Single-Molecule Coherent Modulation Microscopy

Haitao Zhou, Chengbing Qin,* Shuangping Han, Lei Zhang, Ruiyun Chen, Guofeng Zhang, Yaoming Liu, Zhifang Wu,* Sijin Li,* Liantuan Xiao,* and Suotang Jia

Cite This: *Nano Lett.* 2021, 21, 1477−1483 Read Online

ACCESS | Metrics & More | Article Recommendations | Supporting Information

ABSTRACT: Massive magical phenomena in nature are closely related to quantum effects at the microscopic scale. However, the lack of straightforward methods to observe the quantum coherent dynamics in integrated biological systems limits the study of essential biological mechanisms. In this work, we developed a single-molecule coherent modulation (SMCM) microscopy by combining the superior features of single-molecule microscopy with ultrafast spectroscopy. By introducing the modem technology and defining the coherent visibility, we realized visualization and real-time observation of the decoherence process of a single molecule influenced by the microenvironment for the first time. In particular, we applied this technique to observe the quantum coherent properties of the entire chlorella cells and found the correlation between the coherent visibility and metabolic activities, which may have potential applications in molecular diagnostics and precision medicine.

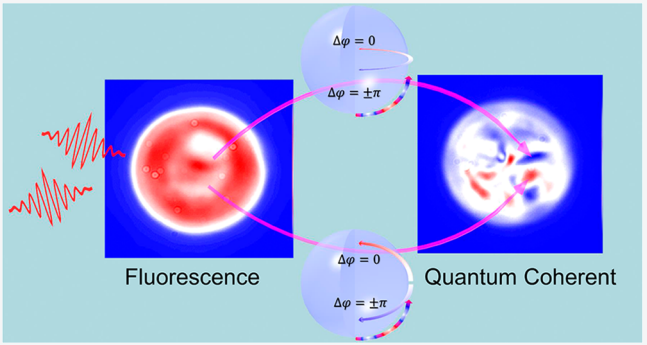

KEYWORDS: *single-molecule microscopy, ultrafast spectroscopy, coherent modulation, quantum coherent imaging, quantum biology*

Microscopy is a powerful tool for humans to observe the microcosm, which helps us understand the origin, development, and death of life.[1] With the reduction of scales in microscopic observation, many novel quantum phenomena have been revealed and discussed.[2−4] For example, researchers have confirmed that the efficient use of solar energy by photosynthesis in green plants is closely related to quantum coherence in both ensemble[5−7] and single light-harvesting complexes.[8,9] In these processes, the microenvironment plays an essential role in maintaining the system quantum correlations in a steady state, which contributes to long-lived quantum coherence in photosynthetic complexes at physiological temperature.[10,11] Some other physiological processes, including energy metabolisms (e.g., respiratory processes[12,13]) and cell canceration,[14−16] are also related to the quantum coherent features of the cells. Investigations of cell physiology and disease pathogenesis heavily rely on untangling the complexity of intracellular quantum coherent mechanisms and pathways. However, demonstrating their quantum coherent features remains a long-standing challenge due to the lack of a useful way to observe the complicated interactions between cells with their local microenvironment. Single-molecule microscopy, not only overcoming the ensemble-averaged effect but also demonstrating good sensitivity to the local microenvironment, is available to study the quantum coherent effects of biological systems. At present, there are two main approaches to investigate the coherent properties at the single-molecule level: absorption and emission spectroscopy. The single-molecule absorption spectrum can directly investigate their coherent properties. However, the absorption cross-section σ of a single molecule at room temperature is 10^6−10^8 times smaller than the area λ^2 of the diffraction-limited spot.[17] Thus, this approach must face a severe background problem in distinguishing the absorption of a single molecule against the fluctuation of the background originating from an incident laser beam.[18−20] In contrast, the single-molecule fluorescence spectrum generally manifests good signal-to-noise and signal-to-background ratios. However, the best results in the fluorescent approach are still achieved by recording the incoherent spontaneous fluorescence emission, rather than coherent processes. Thus, the main challenge to determine the coherent properties by the fluorescent approach is therefore to translate the quantum coherence into the probability of spontaneous emission, which is directly related to the excited-state population probability. Originally, Hulst's

Received: November 24, 2020
Revised: January 24, 2021
Published: January 28, 2021

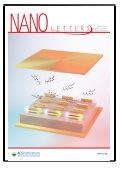

https://dx.doi.org/10.1021/acs.nanolett.0c04626
Nano Lett. 2021, 21, 1477−1483

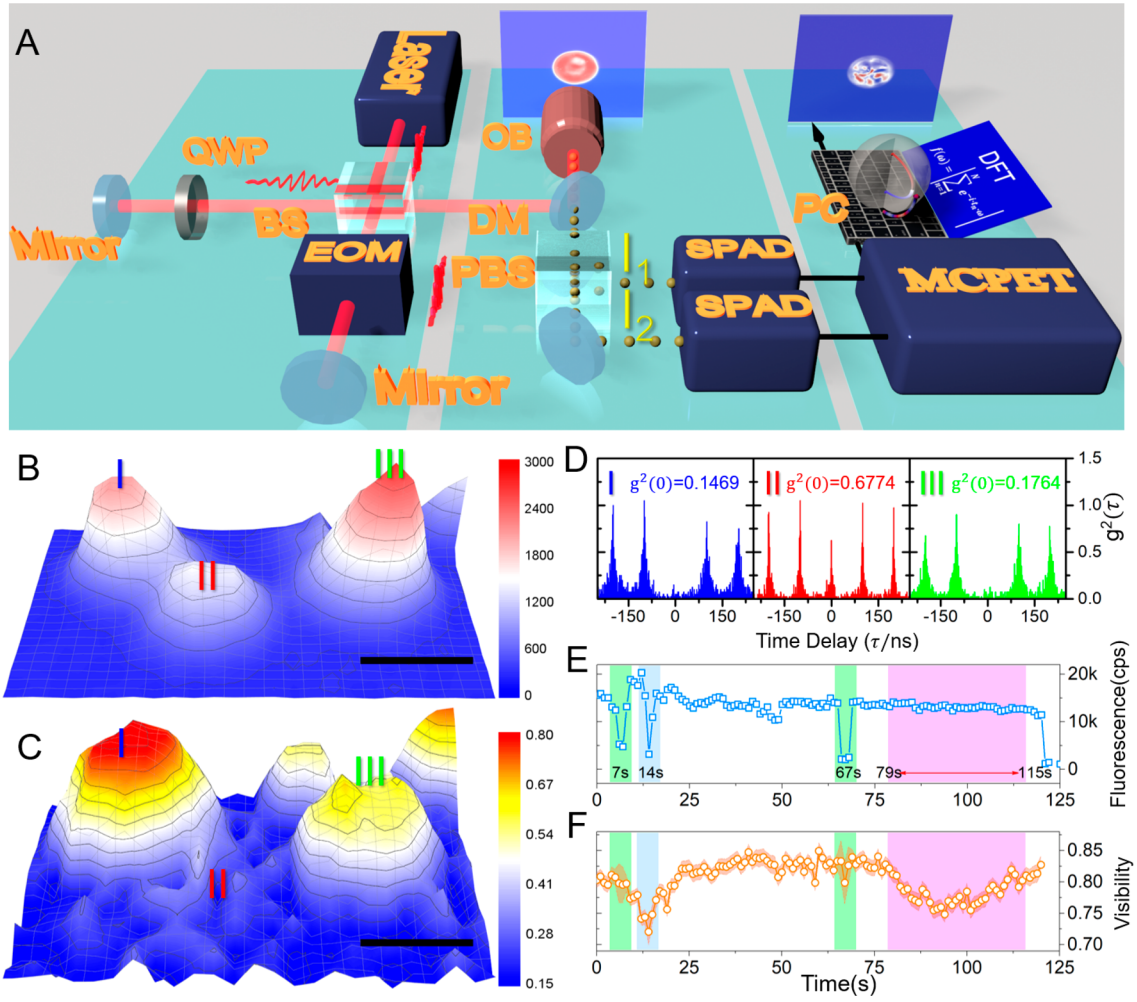

Figure 1. (A) Optical scheme for single-molecule coherent modulation (SMCM) microscopy. Michelson interferometer generates a phase-tunable pulse pair to modulate the coherent state of single molecules. Multichannel picosecond event timer (MCPET, Hydra Harp 400, Pico Quant) records the arrival time of each photon with a picosecond resolution. EOM, electro-optical modulator; QWP, quarter-wave plate; BS, 50/50 beam splitter; DM, dichroic mirror; SPAD, single-photon avalanche diode; PBS, polarization beam splitter. (B) and (C) are the traditional fluorescence imaging and quantum coherent imaging of SR molecules. (I), (II), and (III) are the selected molecules. Scale bars: 0.5 μm. (D) The second-order correlation statistics of the three molecules. (E) is fluorescence intensity trajectory, and (F) is a coherent visibility trajectory with its error bar (the orange shadow) of the single molecule (I). The light green shadows indicate the change only in fluorescence intensities, the light purple shadows indicate the change only in coherent visibilities. The light blue shadow indicates the synchronous variation of both the fluorescence intensity and coherent visibility. The integration time is 1s.

group created, probed, and manipulated the quantum coherent state in single organic molecules and individual light-harvesting complexes at ambient conditions by femtosecond pulse-shaping techniques.[21,22] They demonstrated their quantum coherent information, such as the pure decoherence time T_2^* and Rabi frequency, by fitting the excited-state population probability over the delay time.

These works have made many groundbreaking efforts in obtaining quantum coherent information at the single-molecule level. However, there are still gaps in the visualization and real-time observation of quantum coherence in the entire biological systems. On the basis of our previous work,[23] here we developed the single-molecule coherent modulation (SMCM) microscopy by introducing an innovative approach to visualize the quantum coherent dynamics in a biological microenvironment. Consequently, we revealed the implied relationship between the changes of single-molecule coherent visibility and the metabolic processes of organelles.

In previous work, we developed quantum coherent modulation enhanced single-molecule imaging microscopy (QCME-SMIM), which can improve the contrast of single-molecule imaging by more than 2 orders of magnitude.[23] The giant improvement benefits from the quantum coherent properties of single molecules, combining the ultrafast optics with modem technology. In the scheme, we modulated the excited-state population probability of a single molecule (ρ_{ee}) with a sine wave, $\rho_{ee} \propto 1 + D\cos\Delta\varphi$, by periodically modulating the phase difference ($\Delta\varphi$) between the ultrashort pulse pair. Then we performed a discrete Fourier transform (DFT) of the arrival time of emitted fluorescence photons to determine the magnitude of the Fourier transform. According to our prediction and experimental results, the magnitude of DFT scales linearly with fluorescence photons, emerging a slope factor of ξ. The parameter of D is defined as the modulation depth, which can be calculated by the relationship $D = 2\xi$ (see ref 23 and Derivation-1 in Supporting Information for details).

https://dx.doi.org/10.1021/acs.nanolett.0c04626
Nano Lett. 2021, 21, 1477−1483

The modulation depth D is influenced by both the molecular orientation[23] and decoherence process, expressing as $D = P{\cdot}V$. Here P is the influence factor of the molecular orientation. V is defined as *coherent visibility*, which assesses the influence of the surrounding microenvironment on the decoherence process of a single molecule. A similar visibility function has been defined and approved to extract the decoherence time of a single organic quantum wire isolated in the crystalline matrix recently.[24] In previous work, the frequency domain imaging (i.e., imaging by the magnitude of DFT) presented the combined effect of molecule orientation and coherent visibility; thus the decoherence process of a single molecule cannot be well uncovered. To eliminate the influence of molecular orientation and extract the decoherence process, we designed a polarized beam splitter (PBS) in the detection pathway and determined the fluorescence intensities I_1 and I_2 of single molecules in two perpendicular polarization directions, as shown in Figure 1A. The other experimental procedures are the same as the previous work (see Experimental Setup and ref 23). As we explore in Derivation-2, the orientation of a single molecule can be determined by I_1 and I_2. In this case, the coherent visibility V can be expressed as follows:

$$V = \left(\frac{I_1}{I_2} + \frac{I_2}{I_1}\right)\cdot\xi \tag{1}$$

The coherent visibility allows the characterization of the decoherence process influenced by the interaction between microenvironments and a single molecule. In ideal situations, when a single molecule isolates from the surrounding environment, the population probability of its excited state can be entirely modulated by the phase difference between the ultrashort pulse pair, resulting in $V = 1$. When a single molecule interacts with the surrounding environment, the single molecule's phase information will rapidly lost due to the decoherence process. Consequently, the modulation will be weakened and lead to $V < 1$. As the interaction further increases, V will approach 0.

On the basis of the improved scheme, we carried out both fluorescence intensity imaging and quantum coherent imaging (i.e., imaging the coherent visibility, V), as shown in Figure 1B,C, respectively. Here the fluorescent molecule, Squaraine-derived Rotaxane (SR), was used as a model to reveal the features of our new scheme, due to its good quantum coherent characteristic, high quantum yield, and stable fluorescence intensity (see Sample Preparation).[23] The fluorescence intensity imaging has been illustrated in a three-dimensional (3D) graph in Figure 1B. Note that the intensity order of these three SRs follows III > I > II. This result differs from their coherent visibility in Figure 1C: I > III > II. This difference may result from different interactions, where the coherent visibility is principally affected by the ultrafast processes and the variation of energy levels,[25] while the fluorescence is mainly sensitive to the occurrence of triplet states and the change of conformation structures.[26] Especially for molecule II, it is almost invisible in quantum coherent imaging. Two possible reasons are responsible for this phenomenon, the extremely strong interaction between this single molecule with the surrounding environment and/or more than one molecule located in the laser spot. The latter hypothesis can be confirmed by the second-order correlations ($g^2(0)$) of the three molecules, as shown in Figure 1D. We can find that both molecules I and III show $g^2(0) < 0.5$, indicating only one single molecule is excited. In contrast, $g^2(0) > 0.5$ for molecule II was determined, hinting more than one molecule was within the laser spot. The reduction of coherent visibility can be well understood by considering the anisotropic properties of each molecule and their interaction with the surrounding environments, as the schematic shown in Figure 2A. To assess this

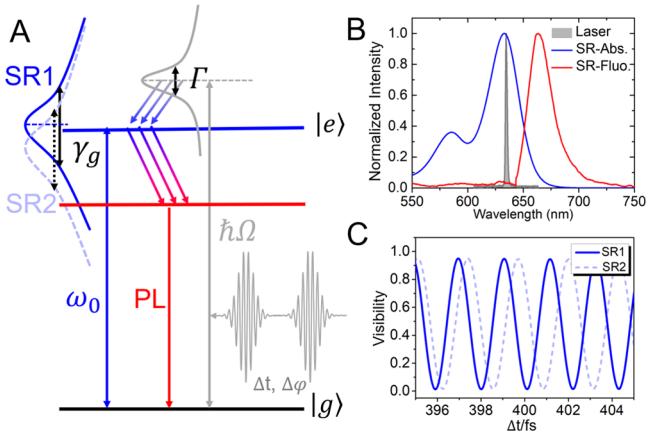

Figure 2. (A) Schematic of the two-level system excited by a phase-controlled laser-pulse pair. γ_g and ω_0 are the line width and frequency of the molecule's absorption spectrum, respectively. The solid and dotted lines represent two different molecules, SR1 and SR2. Γ and Ω are the line width and frequency of incident laser pulse, respectively. (B) Spectral characteristics of the laser pulse and Squaraine-derived Rotaxane molecules (SR, dissolved in dimethyl sulfoxide). (C). Simulated quantum interference signals for two different molecules. The parameters are as follows: $\omega_0 = c/(2\pi \times 630\ \text{nm})$ and $\gamma_g = c \times 10\ \text{nm}/(2\pi \times (630\ \text{nm})^2)$ for SR1 (the solid deep blue line), $\omega_0 = c/(2\pi \times 650\ \text{nm})$ and $\gamma_g = c \times 10\ \text{nm}/(2\pi \times (650\ \text{nm})^2)$ for SR2 (the dashed light blue line), $\Gamma = c \times 2\ \text{nm}/(2\pi \times (635\ \text{nm})^2)$ and $\Omega = c/(2\pi \times 635\ \text{nm})$ for both cases. c is the speed of light.

interpretation, we presented the spectral characteristics of the laser pulse, the excitation, and the fluorescence spectra of SR molecules, as illustrated in Figure 2B. As discussed in the theoretical work by Shin-ichiro Sato[25] and experimental result by Daan Brinks and Richard Hildner,[21,22] the variation of molecule's central frequency (ω_0) and line width (γ_g) would result in different modulation phase. Hence, we simulate the quantum interference signals of two single molecules with the same line width but different central frequencies, as shown in Figure 2C. Note that at the interpulse delay of 400 fs, two single molecules show almost opposite phases, which will lead to the reduction or disappearance of coherent visibility. These results indicate a significant limitation of our approach that low molecule density is desired to gain high-quality quantum coherent imaging and extract the right decoherence information (close to one molecule per diffraction-limited spot is preferred).

To get more insight into the feature of our scheme, we further compared the fluorescence intensity trajectory with the coherent visibility trajectory of molecule I, as shown in Figure 1E,F, respectively. The fluorescence intensity trajectory blinks at 7, 14, and 67 s, and then quenches at 121 s, representing the single molecule character as well as the complex perturbation to the fluorescence intensity. In comparison, coherent visibility trajectory drops at 14 s and perturbs downward around 100 s. Considering the different influential factors, the inconsistency

https://dx.doi.org/10.1021/acs.nanolett.0c04626
Nano Lett. 2021, 21, 1477−1483

between the fluorescence intensity trajectory and coherent visibility trajectory may be interpreted as follows. The fluorescence blinking at 7 and 67 s (in light green shadows) can be ascribed to the occurrence of a triplet state or the formation of dark radical ions, which will lead to a decrease in the quantum yield and a fluorescence blinking,[26] rather than the coherent visibility. The slow drop and recovery of the coherent visibility between 79 and 115 s (in light purple shadows) may be assigned to the change of temperature around the single molecule. While the fluorescence intensity is normally insensitive to the temperature. Furthermore, the fluorescence blinking at 14 s (in light blue shadows) can be assigned to the photoisomerization, which will not only lead to a fluorescence blinking but also result in variations of its structure and energy levels and thus the coherent visibility.

It should be noted that although the single molecule is in a dark state at 14 and 7 s/67 s, the single molecule still presents considerable fluorescence photons. In this case, the coherent visibility still can be determined, although with a relatively large deviation. To evaluate the influence of the photon number on the reliability of the coherent visibility, we performed a numerical simulation based on single-photon modulation[27] (see Simulation-1 in the Supporting Information). We can find that as the photon number increases, the coherent visibility measurements decrease and tends to their true value. Meanwhile, its standard deviations decrease as well. According to the fluorescence intensity, we can obtain the stand deviations of molecule I, as the orange shadow shown in Figure 1F. The small fluctuation determines the effectiveness of our scheme.

Although the variation of quantum features altering by their microenvironment is complex and changeable, the temperature will deterministically affect the quantum coherent properties of single molecules. That is, the lower the temperature, the longer the decoherence time, and thus the higher the coherent visibility. To confirm, we performed measurements on terrylene molecules, which present excellent stability and strong fluorescence intensity at cryogenic and high vacuum conditions (SR generally shows attractive fluorescence characteristics in atmosphere environment with the assistance of oxygen, while almost bleaches under vacuum conditions[28,29]). We measured the coherent visibility of 300 individual molecules of terrylene at different temperatures (17, 31, 50, 100, 200, and 300 K). The averaged values (green balls) and standard deviations (error bars) of coherent visibility at different temperatures are presented in Figure 3. The inset shows the statistical distributions of coherent visibility at the corresponding temperature. We can find that as the temperature increases, the coherent visibility decreases slowly, and its distribution is gradually broadening. These results are consistent with our prediction, as well as other previous works.[22,30−32] To further prove our proposal, we numerically calculated the variation of coherent visibility as the function of temperature through the Liouville equation of a two-level system, as the blue dash-dot shown in Figure 3. Note that the numerical simulation is in good agreement with the experimental data (see Simulation in the Supporting Information and MATLAB Codes 2 for the details).

Finally, we applied quantum coherent imaging to chlorella, which is always used as a model microorganism for studying the photosynthetic apparatus and carbon assimilation.[33,34] Panels A and C of Figure 4 show five successive fluorescence intensity imaging and corresponding quantum coherent

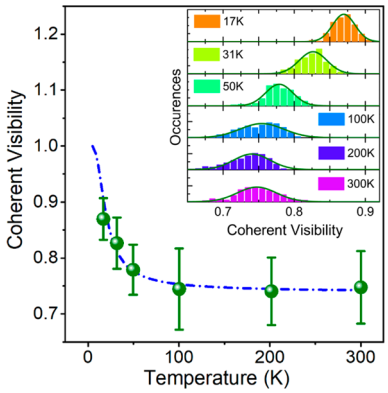

Figure 3. Coherent visibility as a function of temperature. The inset displays the statistic distributions of coherent visibilities of terrylene molecules measured from 17 to 300 K. The green balls are the averaged values, and the error bars are the standard derivation of the distributions. The blue dash line represents the coherent visibility simulated by the Liouville equation of the two-level system.

imaging of SR fluorescently labeled chlorella with an integration time of 20 s. Due to the limitation of the longitudinal resolution of the microscopy system, the fine structure of chlorella and individual molecules are difficult to identify in both images. But they show quite different features: quantum coherent imaging visualizes some tissue structures in the chlorella, which are hidden in the autofluorescence background of chlorella in the fluorescence intensity imaging. This is because SMCM microscopy inherits the ability to improve imaging contrast under an extensive autofluorescence background of QCME-SMIM.[23] Commonly, the visibility of an ensemble system is between 0.01 and 0.1, far less than that of an individual molecule. We suggest that the reduction of visibility in an ensemble system arises from two aspects. One is that an ensemble system's oscillations can be easily averaged out or even entirely removed due to the incoherent superposition between different molecules, as shown in Figure 2C. The other is that the extensive autofluorescence background of chlorella will significantly reduce the modulation amplitude. Although the relatively low coherent visibility, their normalized values still present complicated patterns and rich information, as shown in Figure 4C. To shed more light on the imaging, the subtraction of two adjacent imaging of fluorescence and quantum coherent has been carried out, as presented in Figure 4B,D, respectively. The subtraction from fluorescence intensity imaging shows changes barely, except for fluorescence quenching, while the subtraction from quantum coherent imaging shows a periodical change of the coherent visibility at different positions on the time scales of dozens of seconds (see Figure S3 in the Supporting Information). We speculate that cell metabolic activities,[35] which may vary the local temperatures and the conformational structures of labeled biomolecules and thus the coherent visibility of fluorescent molecules, are associated with the periodic changes. Considering that mitochondria are the main sites of oxidative metabolism in eukaryotes, thus we suggest that the emergence of tissue structure in the quantum coherent imaging can be assigned to the distribution of mitochondria. However, further experiments with specific marks are needed to clarify this conclusion. We also suggest that SMCM might be used to identify cell canceration, which may either be directly derived from amplified uncertainty induced by an increase in quantum

https://dx.doi.org/10.1021/acs.nanolett.0c04626
Nano Lett. 2021, 21, 1477−1483

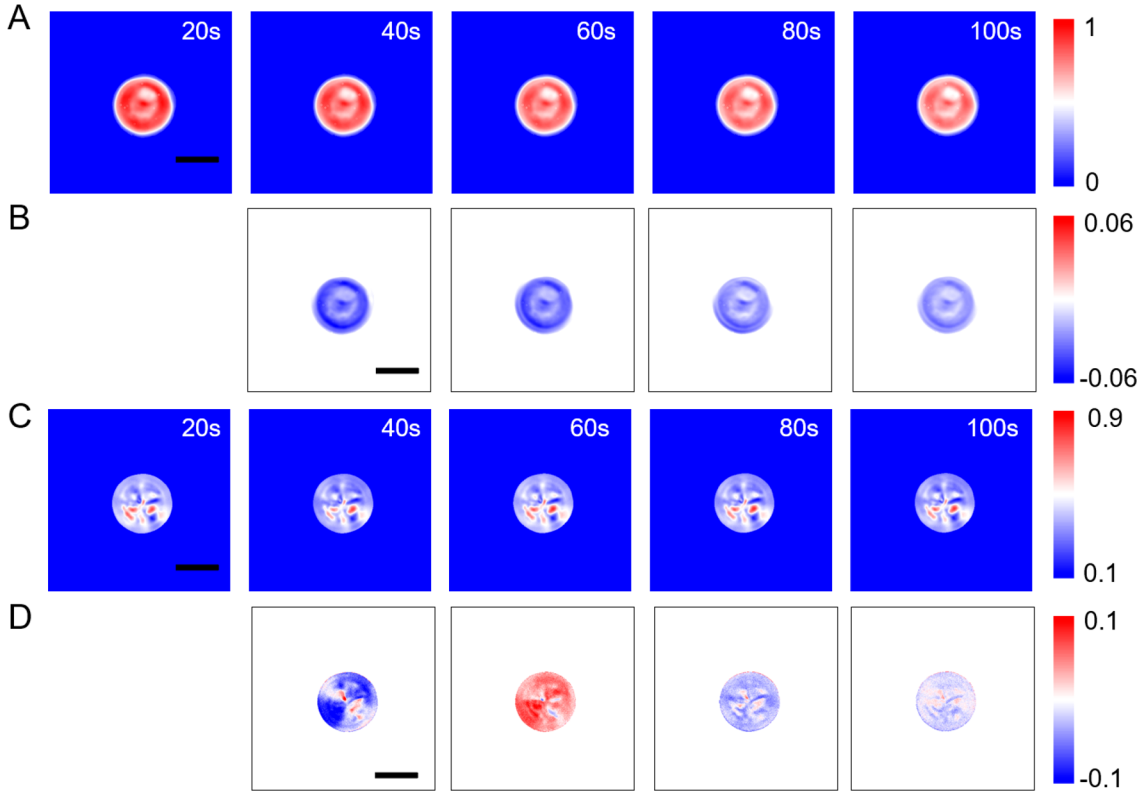

Figure 4. (A) Traditional fluorescence imaging of live chlorella and (C) its quantum coherent imaging showing from 0 to 100 s with an integration time of 20 s. (B) and (D) are subtractions of two successive imaging of (A) and (C), respectively. Scale bars: 5 μm. For clarity and comparability, (A) and (C) are normalized from zero to the maximum values. (B) and (D) represent the ratio of changes in relative physical quantities.

and thermodynamic fluctuation or be indirectly arising from the loss of natural uncertainty reduction mechanisms.[36] To this end, further experiments will be performed by specific labeling, genetic modifications, and more controlled experiments to reveal the direct relationship between these physiological activities and quantum coherent imaging. This approach will provide a new way for cancer diagnosis and a new idea for the study of cell canceration.

In conclusion, on the basis of SMCM microscopy, we realized real-time observation and visualization of single-molecule quantum coherent information both in individual single-molecule and in molecule-labeled living chlorella cells. This research helps us to study the changes of quantum features of organic molecules in the process of cell physiology and then to understand the connection of various metabolic activities, which is of great value for humans to understand life and solve medical problems.

METHODS

Experimental Setup. A tunable subpicosecond laser (FemtoFiber pro TVIS, Toptica) was used to generate ultrashort pulses with a pulse width of 389 fs at 635 nm and 213 fs at 532 nm. The interpulse delay between the two laser pulses was set to 400 fs. The repetition frequency was set to 10 MHz through a pulse picker. Generally, the incident laser power of each pulse was set to 0.1 nJ. The vertically polarized femtosecond laser was split by a beam splitter (BS) to generate two identical laser beams. On one arm, the beam passed through the electro-optical modulator (EOM), while on the other arm, the beam passed through a quarter-wave plate (QWP) to convert the laser into horizontal polarization, as shown in Figure 1A. Thus, two beams recombining at the BS have orthogonal polarizations, which can eliminate the two excitation light pulses interfering with each other. Further details can be found in ref 23.

Sample Preparation. In the experiment, squaraine-derived rotaxanes (SR, MTTI) were used as a model molecule, due to their high quantum yield and excellent stability at room temperature in both air and cell conditions, with the assistance of oxygen.[28,29] Typically, SR molecules, dissolved in dimethyl sulfoxide (DMSO), have a maximum absorption peak at 650 nm and a maximum emission feature at 678 nm (as shown in Figure 2B). Hence, SR molecules were excited with a wavelength of 635 nm. The sample of SR molecules was prepared by spin-coating 20 μL diluted solution (with the concentration of 10^{-10}–10^{-9} M) onto a glass coverslip. Subsequently, the poly(methyl methacrylate) (PMMA) film was spin-coated on the prepared SR molecules to prevent oxidation. The final sample was heated to 373 K under a vacuum for 3 h. Twenty microliters of SR molecules with the same concentration (10^{-10}–10^{-9} M) were dispersed in 1 mL of orella solution for 10 min and then washed with clean water. The chlorella sample was prepared by dropping onto the glass slide. The labeling density in chlorella is estimated to be about 1 per μm^3. On the other aspect, considering that SR molecules generally emerge with strong blinking and weak fluorescence intensity under cryogenic conditions with a high vacuum, we select terrylene molecules to perform temperature-dependent measurements, due to their outstanding features under cryogenic conditions rather than room temperature.[17] Terrylene (UHV equipment) sample was also prepared by spin-coating 20 μL of solution, of which a small quality of

https://dx.doi.org/10.1021/acs.nanolett.0c04626
Nano Lett. 2021, 21, 1477−1483

terrylene (10^{-10}–10^{-9} M) was solved in toluene (3 mg/mL) with a few *p*-terphenyl. Here *p*-terphenyl was used to prevent oxygen-induced fast photobleaching. The terrylene molecule has a maximum absorption peak at 560 nm and a maximum emission feature at 575 nm. Hence, terrylene molecules were excited with a wavelength of 532 nm.

■ ASSOCIATED CONTENT

Supporting Information

The Supporting Information is available free of charge at https://pubs.acs.org/doi/10.1021/acs.nanolett.0c04626.

Derivation-1, derivation of the relationship between the modulation depth D and the slope factor of modulation ξ; Derivation-2, derivation of the coherent visibility V under the weak field approximation; Simulation-1, simulation of the reliability of coherent visibility; Simulation-2, simulation of the Liouville equation of a two-level system; comparison of fluorescence intensity trajectory and coherence visibility trajectory of Chlorella (PDF)

Code 1: Numerical simulation of a random photon number with different modulation coherent factors (ZIP)

Code 2: Numerical solution of the Liouville equation of a two-level system (ZIP)

■ AUTHOR INFORMATION

Corresponding Authors

Chengbing Qin − *State Key Laboratory of Quantum Optics and Quantum Optics Devices, Institute of Laser Spectroscopy, Collaborative Innovation Center of Extreme Optics, Shanxi University, Taiyuan, Shanxi 030006, China;* orcid.org/0000-0002-6822-5113; Email: chbqin@sxu.edu.cn

Zhifang Wu − *Department of Nuclear Medicine, The First Hospital of Shanxi Medical University, Molecular Imaging Precision Medical Collaborative Innovation Center, Taiyuan, Shanxi Province 030001, China*; Email: wuzhifang01@163.com

Sijin Li − *Department of Nuclear Medicine, The First Hospital of Shanxi Medical University, Molecular Imaging Precision Medical Collaborative Innovation Center, Taiyuan, Shanxi Province 030001, China*; Email: lisjnm123@163.com

Liantuan Xiao − *State Key Laboratory of Quantum Optics and Quantum Optics Devices, Institute of Laser Spectroscopy, Collaborative Innovation Center of Extreme Optics, Shanxi University, Taiyuan, Shanxi 030006, China;* orcid.org/0000-0003-2690-6460; Email: xlt@sxu.edu.cn

Authors

Haitao Zhou − *State Key Laboratory of Quantum Optics and Quantum Optics Devices, Institute of Laser Spectroscopy, Collaborative Innovation Center of Extreme Optics, Shanxi University, Taiyuan, Shanxi 030006, China; Department of Nuclear Medicine, The First Hospital of Shanxi Medical University, Molecular Imaging Precision Medical Collaborative Innovation Center, Taiyuan, Shanxi Province 030001, China;* orcid.org/0000-0001-5325-5275

Shuangping Han − *State Key Laboratory of Quantum Optics and Quantum Optics Devices, Institute of Laser Spectroscopy, Collaborative Innovation Center of Extreme Optics, Shanxi University, Taiyuan, Shanxi 030006, China*

Lei Zhang − *State Key Laboratory of Quantum Optics and Quantum Optics Devices, Institute of Laser Spectroscopy, Collaborative Innovation Center of Extreme Optics, Shanxi University, Taiyuan, Shanxi 030006, China*

Ruiyun Chen − *State Key Laboratory of Quantum Optics and Quantum Optics Devices, Institute of Laser Spectroscopy, Collaborative Innovation Center of Extreme Optics, Shanxi University, Taiyuan, Shanxi 030006, China;* orcid.org/0000-0002-0037-856X

Guofeng Zhang − *State Key Laboratory of Quantum Optics and Quantum Optics Devices, Institute of Laser Spectroscopy, Collaborative Innovation Center of Extreme Optics, Shanxi University, Taiyuan, Shanxi 030006, China;* orcid.org/0000-0002-9030-0431

Yaoming Liu − *Scientific Instrument Center, Shanxi University, Taiyuan, Shanxi 030006, China*

Suotang Jia − *State Key Laboratory of Quantum Optics and Quantum Optics Devices, Institute of Laser Spectroscopy, Collaborative Innovation Center of Extreme Optics, Shanxi University, Taiyuan, Shanxi 030006, China*

Complete contact information is available at: https://pubs.acs.org/10.1021/acs.nanolett.0c04626

Author Contributions

C.Q., H.Z., S.L., and L.X. designed and supervised the experiments. H.Z., S.H., and R.C. carried out the optical experiments. Z.W., Y.L., and S.L. are responses for the cell culture. H.Z., L.Z., and G.Z. carried out the simulations. C.Q., H.Z., and S.J. performed the data analysis. All authors have contributed to the manuscript writing and have approved the final version of the manuscript.

Notes

The authors declare no competing financial interest.

■ ACKNOWLEDGMENTS

The authors gratefully acknowledge support from the National Key Research and Development Program of China (Grant No. 2017YFA0304203), Natural Science Foundation of China (Nos. 61527824, 91950109, 62005150, 61875109, 62075120, 62075122, 81671724, 81971655), PCSIRT (No. IRT_17R70), 1331KSC, 1331KIRT, 1331CIC, STIP, OIT, and FSKSC.

■ REFERENCES

(1) Ntziachristos, V. Going Deeper Than Microscopy: The Optical Imaging Frontier in Biology. *Nat. Methods* **2010**, *7*, 603–614.

(2) Cao, J. S.; Cogdell, R. J.; Coker, D. F.; Duan, H. G.; Hauer, J.; Kleinekathofer, U.; Jansen, T. L. C.; Mancal, T.; Miller, R. J. D.; Ogilvie, J. P. Quantum Biology Revisited. *Sci. Adv.* **2020**, *6*, eaaz4888.

(3) Marais, A.; Adams, B.; Ringsmuth, A. K.; Ferretti, M.; Gruber, J. M.; Hendrikx, R.; Schuld, M.; Smith, S. L.; Sinayskiy, I.; Kruger, T. P. J. The Future of Quantum Biology. *J. R. Soc., Interface* **2018**, *15*, 20180640.

(4) Simpson, D. A. Quantum Probes for Biology: Unlocking Single Molecule Dynamics. *Nano Today* **2019**, *24*, 7–9.

(5) Sarovar, M.; Ishizaki, A.; Fleming, G. R.; Whaley, K. B. Quantum Entanglement in Photosynthetic Light-Harvesting Complexes. *Nat. Phys.* **2010**, *6*, 462–467.

(6) O'Reilly, E. J.; Olaya-Castro, A. Non-Classicality of the Molecular Vibrations Assisting Exciton Energy Transfer at Room Temperature. *Nat. Commun.* **2014**, *5*, 3012.

(7) Roscioli, J. D.; Ghosh, S.; LaFountain, A. M.; Frank, H. A.; Beck, W. F. Structural Tuning of Quantum Decoherence and Coherent Energy Transfer in Photosynthetic Light Harvesting. *J. Phys. Chem. Lett.* **2018**, *9*, 5071–5077.

(8) Kondo, T.; Chen, W. J.; Schlau-Cohen, G. S. Single-Molecule Fluorescence Spectroscopy of Photosynthetic Systems. *Chem. Rev.* **2017**, *117*, 860−898.
(9) Hildner, R.; Brinks, D.; Nieder, J. B.; Cogdell, R. J.; van Hulst, N. F. Quantum Coherent Energy Transfer over Varying Pathways in Single Light-Harvesting Complexes. *Science* **2013**, *340*, 1448−1451.
(10) Prior, J.; Chin, A. W.; Huelga, S. F.; Plenio, M. B. Efficient Simulation of Strong System-Environment Interactions. *Phys. Rev. Lett.* **2010**, *105*, 050404.
(11) Panitchayangkoon, G.; Hayes, D.; Fransted, K. A.; Caram, J. R.; Harel, E.; Wen, J. Z.; Blankenship, R. E.; Engel, G. S. Long-Lived Quantum Coherence in Photosynthetic Complexes at Physiological Temperature. *Proc. Natl. Acad. Sci. U. S. A.* **2010**, *107*, 12766−12770.
(12) Nunn, A. V. W.; Guy, G. W.; Bell, J. D. The Quantum Mitochondrion and Optimal Health. *Biochem. Soc. Trans.* **2016**, *44*, 1101−1111.
(13) Dorner, R.; Goold, J.; Heaney, L.; Farrow, T.; Vedral, V. Effects of Quantum Coherence in Metalloprotein Electron Transfer. *Phys. Rev. E* **2012**, *86*, 031922.
(14) Bordonaro, M. Quantum Biology and Human Carcinogenesis. *BioSystems* **2019**, *178*, 16−24.
(15) Uthamacumaran, A. A Biophysical Approach to Cancer Dynamics: Quantum Chaos and Energy Turbulence. *BioSystems* **2017**, *156*, 1−22.
(16) Davidson, R. M.; Lauritzen, A.; Seneff, S. Biological Water Dynamics and Entropy: A Biophysical Origin of Cancer and Other Diseases. *Entropy* **2013**, *15*, 3822−3876.
(17) Moerner, W. E.; Basché, T.; Kurnnzer, S.; Brüchle, C. Low-Temperature Studies in Solids. In *Single-Molecule Optical Detection, Imaging and Spectroscopy*; Basché, T., Moerner, W. E., Orrit, M., Wild, U. P., Eds.; VCH: Weinheim, 1997; pp 34−62.
(18) Chong, S.; Min, W.; Xie, X. S. Ground-State Depletion Microscopy: Detection Sensitivity of Single-Molecule Optical Absorption at Room Temperature. *J. Phys. Chem. Lett.* **2010**, *1*, 3316−3322.
(19) Kukura, P.; Celebrano, M.; Renn, A.; Sandoghdar, V. Single-Molecule Sensitivity in Optical Absorption at Room Temperature. *J. Phys. Chem. Lett.* **2010**, *1*, 3323−3327.
(20) Celebrano, M.; Kukura, P.; Renn, A.; Sandoghdar, V. Single-Molecule Imaging by Optical Absorption. *Nat. Photonics* **2011**, *5*, 95−98.
(21) Brinks, D.; Stefani, F. D.; Kulzer, F.; Hildner, R.; Taminiau, T. H.; Avlasevich, Y.; Mullen, K.; Van Hulst, N. F. Visualizing and Controlling Vibrational Wave Packets of Single Molecules. *Nature* **2010**, *465*, 905−U905.
(22) Hildner, R.; Brinks, D.; van Hulst, N. F. Femtosecond Coherence and Quantum Control of Single Molecules at Room Temperature. *Nat. Phys.* **2011**, *7*, 172−177.
(23) Zhou, H.; Qin, C.; Chen, R.; Liu, Y.; Zhou, W.; Zhang, G.; Gao, Y.; Xiao, L.; Jia, S. Quantum Coherent Modulation-Enhanced Single-Molecule Imaging Microscopy. *J. Phys. Chem. Lett.* **2019**, *10*, 223−228.
(24) Holcman, J.; Al Choueiry, A.; Enderlin, A.; Hameau, S.; Barisien, T.; Legrand, L. Coherent Control of the Optical Emission in a Single Organic Quantum Wire. *Nano Lett.* **2011**, *11*, 4496−4502.
(25) Sato, S. Theory for Quantum Interference Signal from an Inhomogeneously Broadened Two-Level System Excited by an Optically Phase-Controlled Laser-Pulse Pair. *J. Chem. Theory Comput.* **2007**, *3*, 1158−1162.
(26) Stennett, E. M. S.; Ciuba, M. A.; Levitus, M. Photophysical Processes in Single Molecule Organic Fluorescent Probes. *Chem. Soc. Rev.* **2014**, *43*, 1057−1075.
(27) Hu, J.; Liu, Y.; Liu, L.; Yu, B.; Zhang, G.; Xiao, L.; Jia, S. Quantum Description and Measurement for Single Photon Modulation. *Photonics Res.* **2015**, *3*, 24−27.
(28) Wu, R.; Chen, R.; Zhou, H.; Qin, Y.; Zhang, G.; Qin, C.; Gao, Y.; Gao, Y.; Xiao, L.; Jia, S. Detection of Ultra-Low Oxygen Concentration Based on the Fluorescence Blinking Dynamics of Single Molecules. *Appl. Phys. Lett.* **2018**, *112*, 053101.
(29) Li, Y.; Chen, R.; Zhou, H.; Shi, Y.; Qin, C.; Gao, Y.; Zhang, G.; Gao, Y.; Xiao, L.; Jia, S. Observation of Singlet Oxygen with Single-Molecule Photosensitization by Time-Dependent Photon Statistics. *J. Phys. Chem. Lett.* **2018**, *9*, 5207−5212.
(30) Feynman, R. P.; F, L. V., Jr.; Hellwarth, R. W. Geometrical Representation of the Schrödinger Equation for Solving Maser Problems. *J. Appl. Phys.* **1957**, *28*, 49−52.
(31) Allen, L.; Eberly, J. H. *Optical Resonance and Two-Level Atoms*; Courier Corporation: North Chelmsford, 1975.
(32) Palacino-Gonzalez, E.; Gelin, M. F.; Domcke, W. Theoretical Aspects of Femtosecond Double-Pump Single-Molecule Spectroscopy. I. Weak-Field Regime. *Phys. Chem. Chem. Phys.* **2017**, *19*, 32296−32306.
(33) Markou, G.; Dao, L. H. T.; Muylaert, K.; Beardall, J. Influence of Different Degrees of N Limitation on Photosystem Ii Performance and Heterogeneity of Chlorella Vulgaris. *Algal Res.* **2017**, *26*, 84−92.
(34) Polukhina, I.; Fristedt, R.; Dinc, E.; Cardol, P.; Croce, R. Carbon Supply and Photoacclimation Cross Talk in the Green Alga Chlamydomonas Reinhardtii. *Plant Physiol.* **2016**, *172*, 1494−1505.
(35) Shamir, M.; Bar-On, Y.; Phillips, R.; Milo, R. Snapshot: Timescales in Cell Biology. *Cell* **2016**, *164*, 1302−U1235.
(36) Chan, J. Y. On Genetic Information Uncertainty and the Mutator Phenotype in Cancer. *BioSystems* **2012**, *108*, 28−33.

https://dx.doi.org/10.1021/acs.nanolett.0c04626
Nano Lett. 2021, 21, 1477−1483